Theoretical study of *p*- and *n*-type doping of the leucoemeraldine base form of polyaniline: Evolution of the geometric and electronic structure

J. Libert and J. L. Bredas
Service de Chimie des Matériaux Nouveaux, Centre de Recherche en Electronique et Photonique Moléculaires, Université de Mons-Hainaut, Place du Parc, 20, B-7000 Mons, Belgium

A. J. Epstein
Department of Physics and Department of Chemistry, The Ohio State University, Columbus, Ohio 43210-1106
(Received 24 June 1994)

We report quantum-chemical studies on the *p*- and *n*-type doping of the leucoemeraldine base form of polyaniline. The attention focuses on the characterization of the geometric and electronic structure related to the charge-storage species which are formed upon doping. When considering *p*-type doping, which leads to the emeraldine salt form, we find in agreement with previous studies that two polaron- or bipolaron-related bands are induced within the original bandgap. Only the lower of these is deep in the gap and is susceptible to be observed in (photo-)absorption experiments below 3.5 eV. Comparison is made between ring- and nitrogen-centered positive polarons which possess nearly identical stabilities; at low doping level, the two types of polarons induce nearly the same electronic structure; at high doping level, the band structure evolves differently but leads to similar calculated values for the intragap electronic transitions. The geometric and electronic structure obtained for the ring-centered polaron lattice on a single emeraldine salt chain indicates that every other ring adopts a semiquinoid-type geometry and carries most of the unpaired electron density. The characteristics of the positive bipolaron are also investigated; the geometrical results are in close agreement with experiment. In the case of *n*-doping, the negative defects do not correspond to the formation of localized polarons or bipolarons; the geometry modifications are significantly weaker and more extended than in the *p*-doping case. The corresponding band structures are calculated to differ very little from that of the neutral case.

I. INTRODUCTION

Polyaniline represents one of the most important conducting polymers. It has attracted a lot of attention because of its unusual properties (such as doping through acid-base chemistry[1,2]) and wide potential technological applications.[3–5] Polyaniline is a generic term that refers to a family of polymers of general formula

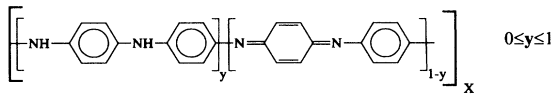

where the nitrogens can be either in a reduced state (amine nitrogens) or in an oxidized state (imine nitrogens). Experimentally, three major forms of polyaniline can be obtained, which differ from one another by the degree of oxidation y (i.e., the ratio of amine nitrogens over the total number of nitrogen atoms):[6,7] (i) the leucoemeraldine base (LEB) form, where $y=1$; (ii) the emeraldine base (EB) form, where $y=0.5$; and (iii) the pernigraniline base (PNB) form, where $y=0$. These polymers can also exist in the corresponding protonated (salt) form. Emeraldine salt (ES) is the highly electrically conducting form of polyaniline. The largest conductivity reported to data is on the order of 400 S/cm;[8] this value is some 14 orders of magnitude higher than in the insulating emeraldine base form. The insulator-to-conductor transition can be simply triggered by protonation (acid-base chemistry) of the EB form, a process which does not modify the number of electrons along the chains.[9] Many studies performed on ES suggest that the metallic state of this polymer is related to the formation of a polaronic lattice.[9–12]

As is the case with the other conducting polymers,[13,14] polyaniline also can reach the highly conducting metallic state following a redox process (which modifies the number of electrons within the chains).[15] The oxidation of leucoemeraldine base, which is an insulator, first leads to the highly conducting emeraldine salt; further oxidation results in the pernigraniline oxidation state, which is also insulating. In this context, the emeraldine salt constitutes a conducting window along the oxidation path.[16,17]

The insulator-metal transition of polyaniline obtained by protonation of emeraldine base (with acids such as HCl) and oxidation of leucoemeraldine base (by, for example, Cl_2) involves strong electron-phonon coupling, i.e., interconnection between the geometric structure and electronic structure of the polymer.[9–11,18,19] The electron-phonon coupling manifests itself through not only bond-length dimerization aspects[20,21] but also ring-torsion dimerization considerations.[22,23] The influence of ring torsions[22–26] appears to be a key aspect in the large effective masses observed for the charge-storage species in polyaniline.[27–29]

In this work, we present a quantum-chemical study of both *p*- and *n*-type doping of leucoemeraldine base, the fully reduced form of polyaniline. We characterize the geometric and electronic structure of the charge-storage

species which appear on doping; we compare our results to those of experimental (normal and photoinduced absorptions, x-ray diffraction) studies. We are able to provide a complete description of the charge-storage species (in a context where we do not consider interchain effects or Coulomb interactions with doping species) and, in particular, propose a refined picture of the polaron lattice in an emeraldine salt chain.

II. METHODOLOGY

We use the Hartree-Fock semiempirical Austin model 1 (AM1) technical to perform geometry optimizations of the ground state of a model LEB oligomer, in the neutral, *p*-doped, and *n*-doped states. AM1 is parametrized to reproduce ground-state geometries and heats of formation of organic molecules.[30,31] It also provides much more accurate torsion-angle estimates than its predecessor, the modified neglect of differential overlap (MNDO) technique.[32,33] The model oligomer we have chosen to work with is a phenyl-capped tetramer (since it actually contains five phenyl rings, we loosely refer to it as a pentamer; see Fig. 1); this oligomer represents the best compromise between chain length (which we try to have as large as possible) and computer time requirements. We have avoided considering oligomers with terminal amine ($-NH_2$) groups; indeed, such terminal groups, which are π donors, tend to overly attract the positive charges formed during *p*-type doping. Note also that the counterions have not been taken into account. In some cases, calculations have also been performed on longer oligomers in order to better describe some particular defects.

Three different approaches are used to perform the AM1 geometry optimizations, depending on the kind of charge-storage species under consideration. Since the neutral and bipolaron cases correspond to closed-shell systems, these are optimized at the restricted Hartree-Fock (RHF) level. In contrast, the singly charged (*p*- or *n*-doped) oligomers, are optimized at the restricted open-shell Hartree-Fock (ROHF) level as well as in some cases at the unrestricted Hartree-Fock (UHF) level [note that the latter two methods, which are better suited to represent systems with unpaired electron(s), are more costly in computing time than the RHF technique].[34,35] We have also taken an UHF or ROHF–configuration-interaction (CI) approach to study an oligomer containing two positive charges; in that case, we are able to simulate the formation of two radical cations (polarons), while a RHF approach on the same system would allow for the formation of a dication (bipolaron). It must be noted that the ROHF-CI approach (as implemented in the MOPAC package) allows for the optimization of molecules which could present a biradical character; it consists in an open-shell treatment coupled to a multielectron configuration-interaction calculation (MECI).[36]

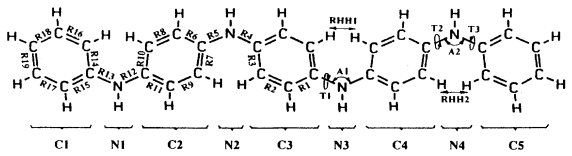

FIG. 1. Sketch of the LEB pentamer; the labels are those referred to in the tables.

During the geometry optimization procedure, all the bond lengths and bond angles are fully optimized. To be consistent with the results of x-ray diffraction experiments, all the nitrogen atoms are considered to be in the same plane.[25,37] Some geometric constraints, supported by preliminary AM1 and *ab initio* 3-21G calculations, are also imposed; all the *para* carbon atoms and the hydrogens linked to the amine sites are coplanar with the nitrogens (which are therefore of sp^2 character) and all the carbons of a ring define a single plane. The only torsion angles that need to be optimized, therefore, are those between each of the phenyl rings and the plane of the nitrogen atoms. No inversion symmetry is imposed; however, we found that the optimized geometries of all pentamers (neutral and charged) present an inversion center (see Fig. 1).

For *p*-doped and *n*-doped oligomers, we consider singly and doubly charged systems. The net atomic charges are calculated and compared to those obtained in the neutral case. In this way, the geometry optimizations provide the geometric representation of, and the charge distribution in, the different charge-storage species that appear upon *p*- or *n*-type doping of LEB.

From the geometric structures obtained for the oligomers in different charged states, it is possible to build unit cells that are representative of different doping levels of the leucoemeraldine polymer chain. Based on these unit cells, we then apply the valence effective Hamiltonian (VEH) technique[38,39] to calculate the electronic band structures of single LEB chains in the neutral and doped states. The VEH technique is well known to provide accurate values for bandwidths and ionization potentials and also leads to good estimations of band gaps in conjugated polymers.

We note that the same methodological approach has already been successfully followed in a previous study on the polyaniline base forms.[26]

In order to compare the stabilities of the different charged species in LEB and some other more conventional intrinsic conducting polymers [for example, *trans*-polyacetylene, polythiophene, and poly(*para*phenylene-vinylene)], we have calculated the defect binding energies at the AM1 level. These AM1 values have been shown to be much higher than those obtained experimentally[40] or by simple Su-Schrieffer-Heeger (SSH) Hamiltonian approaches,[41] but are expected to provide good relative trends.

III. RESULTS AND DISCUSSION

The notations used to describe the optimized geometrical parameters collected in Tables I and III and the groups of atoms for which the net atomic charge distributions are reported in Tables II and IV are illustrated in Fig. 1.

TABLE I. Geometries in the neutral (AM1-RHF), (+1)-charged (AM1-UHF), and (+2)-charged (AM1-UHF and AM1-RHF) states of the LEB pentamer. The modifications Δ relative to the neutral system are also indicated. The bond lengths (Rx) and the distances between interacting hydrogen atoms ($RHHx$) are in Å. The bond angles and torsion angles (Ax and Tx) are in degrees. The labels are given in Fig. 1.

Parameter	Neutral (RHF)	+1 (UHF)	Δ+1 (UHF)	+2 (UHF)	Δ+2 (UHF)	+2 (RHF)	Δ+2 (RHF)
$R1$	1.412	1.435	+0.023	1.416	+0.004	1.450	+0.038
$R2$	1.386	1.366	−0.020	1.390	+0.004	1.355	−0.031
$R3$	1.415	1.440	+0.025	1.419	+0.004	1.457	+0.042
$R4$	1.396	1.361	−0.035	1.406	+0.010	1.345	−0.051
$R5$	1.397	1.402	+0.005	1.367	−0.030	1.384	−0.013
$R6$	1.412	1.419	+0.007	1.433	+0.021	1.432	+0.020
$R7$	1.415	1.421	+0.006	1.438	+0.023	1.433	+0.018
$R8$	1.386	1.383	−0.003	1.370	−0.016	1.367	−0.019
$R9$	1.386	1.384	−0.002	1.369	−0.017	1.367	−0.019
$R10$	1.415	1.428	+0.013	1.443	+0.028	1.443	+0.028
$R11$	1.411	1.421	+0.010	1.439	+0.028	1.436	+0.028
$R12$	1.398	1.380	−0.018	1.357	−0.041	1.352	−0.046
$R13$	1.394	1.404	+0.010	1.408	+0.014	1.419	+0.025
$R14$	1.417	1.417	0.000	1.420	+0.003	1.412	−0.005
$R15$	1.415	1.415	0.000	1.418	+0.003	1.410	−0.005
$R16$	1.389	1.392	+0.003	1.391	+0.002	1.391	+0.002
$R17$	1.319	1.394	+0.003	1.393	+0.002	1.393	+0.002
$R18$	1.393	1.395	+0.002	1.398	+0.005	1.395	+0.002
$R19$	1.395	1.398	+0.003	1.401	+0.006	1.396	+0.001
$T1$	26.4	18.6	−7.8	41.5	+15.1	20.2	−6.2
$T2$	−30.0	−28.4	+1.6	−11.9	+18.1	−18.0	+12.0
$T3$	25.0	29.3	+4.3	38.8	+13.8	41.6	+16.6
$A1$	125.5	128.3	+2.8	126.8	+1.3	131.8	+6.3
$A2$	125.9	125.3	−0.6	127.4	+1.5	125.4	−0.5
$RHH1$	2.323	2.081	−0.242	2.272	−0.051	1.902	−0.421
$RHH2$	2.283	2.362	+0.079	2.187	−0.096	2.428	+0.145

A. Neutral state

1. *Geometric and electronic structure of the neutral pentamer*

The AM1-RHF optimized geometrical parameters for the ground-state geometry of the neutral pentamer are presented in Table I. All the rings adopt an aromaticlike geometry, i.e., the carbon-carbon bond lengths within the rings are equivalent (within 0.030 Å). The ring torsion angles alternate in sign and are on the order of 25°–30°. The calculated torsion angles obtained for LEB appear to be smaller than those estimated using x-ray diffraction results for partially crystalline materials (on the order of 40°).[42] The AM1-RHF results agree with the common representation of LEB as having no effective bond-length dimerization and no torsion-angle dimerization.[25,26] The

TABLE II. Net atomic charge distributions for the neutral (AM1-RHF), singly positively charged (AM1-UHF), and doubly positively charged (AM1-UHF and AM1-RHF) states of the LEB pentamer. The modifications Δ relative to the neutral state are also indicated. All the net atomic charges are in $|e|$. The labels are given in Fig. 1.

Group	Neutral	+1 (UHF)	Δ+1 (UHF)	+2 (UHF)	Δ+2 (UHF)	+2 (RHF)	Δ+2 (RHF)
$C1$	0.028	0.091	+0.063	0.265	+0.237	0.198	+0.170
$N1$	−0.071	−0.022	+0.049	0.217	+0.288	0.083	+0.154
$C2$	0.080	0.150	+0.070	0.356	+0.276	0.274	+0.194
$N2$	−0.071	0.144	+0.215	0.055	+0.126	0.269	+0.340
$C3$	0.070	0.272	+0.202	0.220	+0.150	0.360	+0.290
$N3$	−0.071	0.144	+0.215	0.055	+0.126	0.269	+0.340
$C4$	0.080	0.150	+0.070	0.356	+0.276	0.274	+0.194
$N4$	−0.071	−0.022	+0.049	0.217	+0.288	0.083	+0.154
$C5$	0.028	0.091	+0.063	0.265	+0.237	0.198	+0.170

net atomic charge distributions in the neutral pentamer are given in Table II. There occurs a very slight alternation between the net charges carried by the rings ($+0.07|e|$) and those of the amine groups ($-0.07|e|$).

Results obtained from VEH oligomeric calculations on the trimer, tetramer, pentamer, hexamer, and dodecamer show that the transitions from highest occupied to lowest unoccupied molecular orbitals (HOMO-LUMO) (π-π^*) are 4.47, 4.16, 4.05, 3.98, and 3.86 eV, respectively; this decrease in π-π^* transition is in accord with the extension of the conjugated path when increasing the oligomer size. Extrapolation of the oligomer transitions would lead to a 3.70 eV band gap for the polymer.

2. *Electronic structure of the LEB polymer chain*

The translation unit cell used to calculate the VEH electronic band structure of LEB has been built from the center of the neutral pentamer. It consists in two -NH-ring- units, each formally containing eight π electrons. The band structure is given in Fig. 2. Although the main characteristics of the band structure have already been discussed previously,[19,23,26,43] it is important to recall the following points. The bands are degenerate two by two at the end of the first Brillouin zone due to the presence of a glide-plane symmetry within the unit cell.[19] The HOMO and LUMO bands possess very different widths, 2.83 and 0.16 eV, respectively. The π-π^* transition between the HOMO and LUMO bands is calculated to occur at 3.81 eV, which is in good agreement with the experimental values (3.6–3.8 eV),[44] and with the extrapolation from the calculated band gaps for the oligomers.

The markedly different electronic characteristics of the

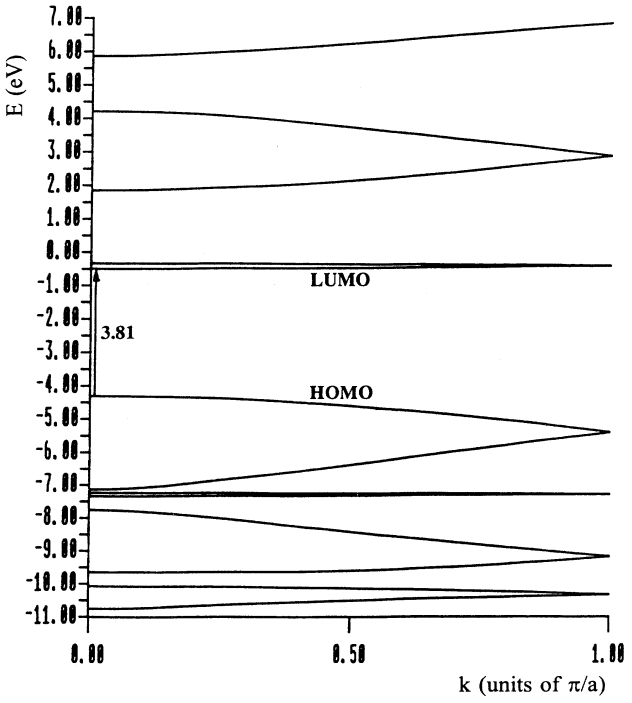

FIG. 2. VEH electronic band structure of the neutral LEB chain.

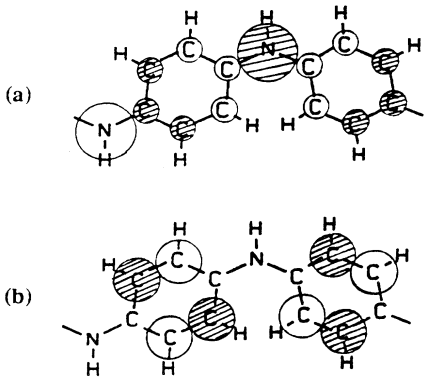

FIG. 3. Illustration of the VEH LCAO π coefficients for (a) the HOMO and (b) the LUMO of leucoemeraldine base.

HOMO and LUMO bands are exemplified in Fig. 3 by the corresponding linear combination of atomic orbitals (LCAO) π coefficients. For the HOMO (top of the valence band), all the carbon and nitrogen atoms present significant LCAO π coefficients, with a bonding-antibonding pattern characteristic of aromatic systems; this denotes important π delocalization along the polymer chain, which gives rise to a large bandwidth. In the case of the LUMO (bottom of the conduction band), there are significant LCAO π coefficients only on the *ortho*-carbon atoms; nodes in the wave function are present on the nitrogen and *para* carbon atoms; π interaction between units is therefore strongly prevented, which explains the flatness of the band. This very large electron-hole asymmetry leads us to expect, from the very beginning, different modifications for *p*- and *n*-doped leucoemeraldine chains.

B. *p*-doped pentamer: Single-polaron formation

1. *Geometric and electronic structure of the (+1)-charged pentamer*

The (+1)-charged pentamer has been optimized using the AM1-ROHF and AM1-UHF techniques; both lead to very similar geometries.

The optimized geometrical parameters for the (+1)-charged molecule are presented in Table I. The structural modifications induced by the introduction of a single positive charge correspond to the formation of a positive polaron $P^{+\cdot}$; they mainly occur in the center of the oligomer and particularly on the central phenyl ring (see $R1$, $R2$, and $R3$ in Table I) and the adjacent C-N bonds ($R4$). This part of the molecule adopts a semiquinoidlike geometry which is intermediate between aromatic and quinoid geometries [r(C*p*-N)=1.361 Å; r(C*p*-C*o*)=1.438 Å; and r(C*o*-C*o*)=1.366 Å; note that C*p* and C*o* refer to *para* and *ortho* carbon]. The remaining bonds of the oligomer are only slightly affected; some modifications are, however, observed on the most external C-N bonds ($R12$ and $R13$) and some of the adjacent C*p*-C*o* bonds ($R10$ and $R11$). The external rings are not affected. The bond-length modifications can be roughly sketched in the following way:

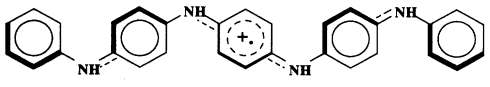

Turning to the ring torsion angles, we observe that the one associated with the central ring is modified most significantly; this phenyl ring gets closer to the plane of the nitrogen atoms ($T=18.6°$ at the UHF level and 16.0° at the ROHF level, instead of 26.4° calculated for the neutral case); this is also true for the adjacent rings but to a lesser extent, while the external rings rotate slightly away from the nitrogen plane.

The evolution in the inner C-N-C bond angles ($A1$) is related to the more coplanar configuration adopted by the three internal phenyl rings. This new configuration induces an increase in the steric interactions between *ortho* hydrogen atoms of these rings (see the evolution of $RHH1$ in Table I), which is partly compensated by a larger value of the C-N-C bond angle $A1$. The external C-N-C bond angles ($A2$) undergo a slight decrease because the dihedral angle between the rings they connect increases by about 3°. [Note that the van der Waals radius of a hydrogen atom is generally considered to be 1.2 Å (Ref. 45).]

The geometry-optimization results on the pentamer, when extrapolated to the polymer, suggest that upon extracting one electron, a positive polaron $P^{+\cdot}$ is formed on the chain, which is essentially localized on one phenyl ring and the adjacent nitrogens. This situation implies that the positive polaron is more confined than previously estimated on the basis of results obtained within the Su-Schrieffer-Heeger approach assuming only ring torsion-angle changes.[22,23] The analysis of the charge distributions in the (+1)-charged oligomer (see Table II) is consistent with this picture of stronger localization. Indeed, with respect to the neutral case, the positive charge is seen to be mainly localized in the center of the oligomer. In fact, about 63% of that charge is concentrated on the central phenyl ring and the neighboring amine sites at the AM1-UHF level (53% at the AM1-ROHF level). The other parts of the oligomer gain much smaller portions of the positive charge.

If we compare these LEB results with those obtained for polythiophene (PT) and *trans*-polyacetylene [*trans*-$(CH)_x$] oligomers of similar lengths (24 linked carbon atoms along the conjugated path), the extension of the positive polaron is found to be similar in all these cases; such a defect extends over about 18 sites along the chain for *trans*-$(CH)_{24}$, sexithiophene, and the LEB pentamer; the situation is also similar in poly(*p*-phenylene vinylene) (PPV) where the positive polaron is spread over about 22 sites along the chain of a pentamer (28 carbons long). This similarity might appear to be surprising if we consider that, in contrast to the other systems, polyaniline possesses an additional degree of freedom, ring torsion, which contributes to decrease the delocalization along the chain. However, whereas the other conjugated polymers present geometrical relaxations that decrease smoothly when going toward the edges of the defect, the LEB pentamer has its phenyl rings adjacent to the center of the defect that are little affected, the geometric deformations being almost localized on their external C-N bonds. The AM1-ROHF binding energy for the positive polaron in the LEB pentamer is 0.22 eV (identical for the AM1-UHF approach) as compared with 0.17, 0.24, and 0.31 eV calculated for the PPV, PT, and *trans*-$(CH)_x$ oligomers, respectively; these results suggest that the geometric relaxation is as strong in LEB as in PT and a little bit lower than for *trans*-$(CH)_x$, which can be related to the presence of aromatic structures along the polymer chain.

We note that, in order to best characterize the positive polaron, we have also optimized at the AM1-ROHF level a longer phenyl-capped oligomer which contains six rings. The geometrical deformations are nearly identical to those observed for the pentamer, but leads to a non-symmetric defect which presents nitrogen-centered polaron characteristics from bond-length and torsion-angle viewpoints. It should be borne in mind that, in previous instances,[9,11,22,23] the polaron has often been depicted as being centered on a nitrogen atom and not on a ring. In order to clarify this situation, we have optimized phenyl-capped tetramer and hexamers where we did or did not impose a symmetry plane centered on the nitrogen atom in the middle of the system. The ROHF optimized geometry of the singly doped LEB tetramer is presented in Fig. 4 for the symmetric case; there, the positive charge induces the formation of a polaron centered on the central nitrogen atom which is surrounded by two phenyl rings of semiquinoid geometry. In comparison to the neutral case, both of these rings adopt a smaller torsion angle (±20.0° vs ±28.5°), while the neighboring rings reach larger ones (±40.0° vs 26.0°) and present only slight bond-length deformations. The nitrogen-centered polaron is only 0.24 kcal/mol less stable than the ring-centered polaron; such a total energy difference of +0.24 kcal/mol (0.01 eV/polaron) is not significant. In the case of the hexamer, the difference is of 0.52 kcal/mol. Thus, depending on external conditions, either one of these polaron topologies could be present.

In order to understand the relative influence of the torsion-angle and bond-length relaxations on the polaron

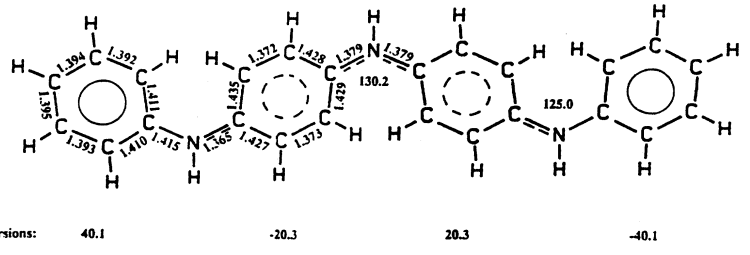

FIG. 4. AM1-ROHF optimized geometry of the LEB tetramer supporting a N-centered positive polaron. The bond lengths are in Å. The bond and torsion angles are in degrees.

configuration, we have also performed geometry optimizations of the (+1) pentamer where we kept fixed, as in the neutral case, (i) the whole geometry, (ii) only the torsion angles, and (iii) only the bond lengths; from the results, we can conclude that, upon (+1) doping, the torsion-angle and bond-length contributions to the total polaron relaxation (0.22 eV) are on the order of 20% and 80%, respectively.

VEH oligomer calculations performed on the (+1)-doped LEB pentamer show that only one polaron level appears deep within the π-π^* gap; it is destabilized by about 0.34 eV in comparison to the HOMO level of the neutral pentamer (0.30 eV for the hexamer), a value similar to that obtained for the PPV pentamer (0.31 eV). For the (+1)-charged LEB pentamer, the VEH transition from the new HOMO level to the first polaron level is calculated at 0.95 eV; it evolves to 0.72 eV for the ring-centered polaron in the LEB hexamer (0.69 eV for the nitrogen-centered polaron). The second polaron level remains at the very edge of the conduction band, due to its wave-function characteristics. The transition between the polaron levels is at 3.70 eV for both oligomers.

2. *Electronic structure of the 25% p-doped LEB*

From the optimized geometries of the (+1)-charged pentamer and symmetric (+1)-charged hexamer, it is possible to extract unit cells which contain four -(NH-ring)- units and one positive polaron $P^{+\cdot}$ centered either on a phenyl ring or on a nitrogen atom. These unit cells correspond to 25% p-doped LEB chains; the corresponding VEH band structures are displayed in Fig. 5. Note that, relative to the neutral case (Fig. 2), there appear twice as many bands since the unit cells are twice as large. Due to the disappearance of the glide-plane symmetry along the chain, there are no longer any degeneracies at either the first Brillouin zone edge or the zone center. With respect to the leucoemeraldine base band structure, we obtain that the original upper occupied (HOMO) band evolves into four distinct bands, the highest of these being only half occupied.

From the band structure in Fig. 5(a) (ring-centered positive polaron), we can consider that two polaron bands are formed in the gap: (i) the lower polaron band P_a (half filled) is 0.19 eV wide and lies 0.35 eV above the valence band edge; (ii) the upper polaron band P_b (empty) is extremely flat (0.004 eV wide) and lies 0.06 eV below the conduction band. As a consequence of the electron-hole asymmetry in leucoemeraldine, the two polaron bands are thus markedly different; only the lower one is well defined in the gap, in agreement with experimental observations of two intragap absorptions.[11,46]

VEH transitions below 4.0 eV which involve the lower polaron band P_a and the valence bands are calculated at 0.7, 1.6, 2.6, and 3.1 eV. Up to now, the investigation of the LEB p doping has mainly been performed electrochemically. The VEH theoretical transition values agree well with the optical absorption measurements carried out for electrochemically doped polyaniline films by Monkman *et al.*;[47] for an oxidation potential [0.2 V vs the standard calomel electrode (SCE)] intermediate between LEB and ES, these authors observed three features at 0.57, 1.31, and 2.51 eV. This suggests that at 0.2 V vs SCE the polyaniline state might correspond to approximately 25% oxidized LEB chains. From Fig. 5(b), it is worth noting that the nitrogen-centered positive polarons induce nearly the same electronic structure as the ring-centered polarons; this emphasizes the similarity of the relaxation energies for the two types of positive polarons.

Since, at a 25% level of p doping, the lower polaronic band remains rather narrow [which suggests weak interactions (overlap) between positive polarons], a qualitative comparison could be made with photoinduced absorption experiments in which the excited species are generally well separated; even though there seems to be a good agreement, some caution must be used here because the VEH-calculated transitions depend strongly on the doping level. In photoinduced experiments, three photoinduced peaks are observed at 0.75, 1.4, and 2.8 eV.[44] The 0.75 and 2.8 eV peaks have been attributed to the formation of positive polarons[22,23] while the 1.4 eV peak has a different nature (and behavior) and has been con-

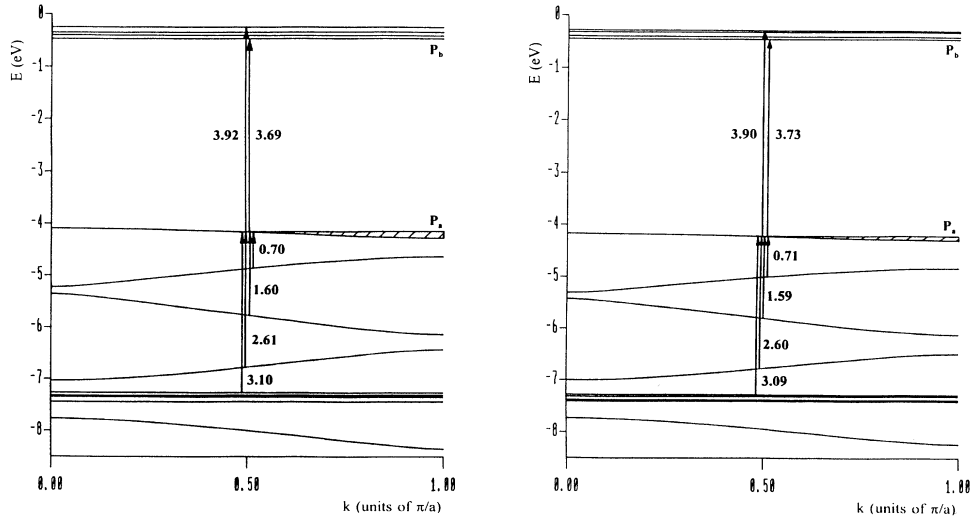

FIG. 5. VEH electronic band structure of the 25% p-doped LEB chain containing (a) ring-centered and (b) nitrogen-centered polarons.

sidered as coming from positive polarons trapped by residual quinoid units along the LEB chain.[44]

Within a Hückel-like SSH approach, Ginder and Epstein[22,23] have obtained a polaron level in the gap with a transition from the valence band to this level and a transition from this level to the conduction band corresponding to 0.75 and 2.8 eV, respectively; they associated these transitions with the photoinduced peaks. However, valence effective Hamiltonian results indicate that no absorption below 3.5 eV should involve the second polaron band or the conduction bands; in the oligomer and polymer calculations, the transition between the two polaron levels is in general larger than or equal to 3.7 eV. In the framework of the VEH results, the observed intragap transitions rather imply valence bands and the first polaron level. Previous results obtained by Stafström *et al.* also support this interpretation.[11]

C. *p*-doped pentamer: Formation of two polarons

1. *UHF geometric and electronic structure of the (+2)-charged pentamer*

We have investigated the pentamer with two positive charges both at the UHF and ROHF-CI levels. This allows us to take into account the formation of two separate radical cations, i.e., two polarons. The AM1-UHF optimized geometry of the (+2)-charged pentamer is presented in Table I. Relative to the neutral case, the +2 charge leads at the UHF level to a strong geometric evolution, mainly around phenyl rings $C2$ and $C4$ and the adjacent C-N bonds ($R5$ and $R12$) which all correspond to a semiquinoid geometry [r(Cp-N)=1.367 Å, r(Cp-Co)=1.435 Å, and r(Co-Co)=1.370 Å]. Smaller modifications take place on the next-nearest C-N bonds ($R4$ and $R13$). In the ROHF-CI optimization, the C-N bonds $R5$ and $R12$ are more strongly affected while the modifications of the inner-ring bond lengths are similar.

Compared to the singly charged case, all the torsion angles along the oligomer are strongly modified. The $C2$ and $C4$ rings become much more coplanar to the nitrogen-atom plane with torsion angles of −11.9° (−3.6° in ROHF-CI). In contrast, the central phenyl ring moves strongly out of this plane (torsion angle of 41.5°; 54.6° in ROHF-CI) as is also the case for the external phenyl rings (torsion angles of 38.8°). The rotation of the central and external rings prevents strong steric interactions from occurring with the two semiquinoid rings. With respect to the neutral case, the dihedral angles between neighboring rings ($T1+|T2|$ and $|T2|+T3$) have slightly decreased by 3°–5°. Simultaneously, the C-N-C bond angles (see $A1$ and $A2$) increase in order for the interacting hydrogen atoms (see $RHH1$ and $RHH2$) to be further away from one another. We note that the ROHF-CI approach leads to a stronger torsion-angle dimerization, while the UHF method gives here more delocalized defects.

The AM1-UHF net atomic charge distributions for the (+2)-charged pentamer are presented in Table II; major increases in positive charge occur on the left- and right-hand sides of the system, while smaller values are found in the center. This indicates that the +2 charge has split into two single positive charges localized on different sites of the pentamer. In fact, phenyl ring $C2$ and the adjacent amine groups support 70% of a single +1 charge; the situation is equivalent for ring $C4$. If we include the contribution from the phenyl ring $C1$ ($C5$), one finds 93% of a +1 charge (it must be noted that the ROHF-CI technique leads to very similar results with differences of only a few percent). This situation thus corresponds to the formation of two positive polarons $P^{+\cdot}$ centered on two different phenyl rings along the oligomer. Note that the gain in positive charge around each defect is not symmetric; this is due to Coulomb repulsion between the two positive polarons, which induces a slightly larger charge on the more external amine units.

Figure 6 illustrates the UHF LCAO π coefficients for the HOMO α and β orbitals of the doped pentamer, which are each associated with a radial (cation). These orbitals are mainly localized on phenyl rings $C2$ and $C4$ and the adjacent nitrogen atoms of the pentamer, respectively; this is in total agreement with the localization of the geometric deformations described above.

The AM1-UHF (and AM1-ROHF-CI) results for the LEB pentamer supporting two positive polarons can be extrapolated to the 50% oxidized LEB, i.e., the polaron lattice in emeraldine salt. In this framework, the unit cell contains two phenyl rings; one of them carries a positive

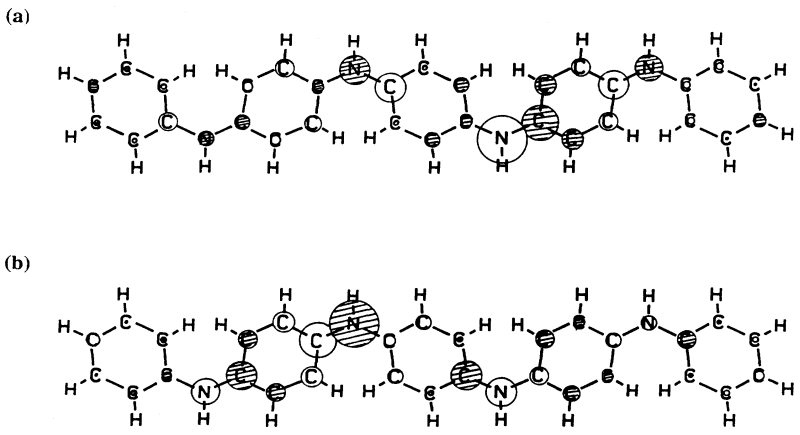

FIG. 6. Illustration of the AM1 LCAO π coefficients for (a) the α HOMO and (b) the β HOMO of the doubly charged (AM1-UHF) LEB pentamer.

polaron and possesses a semiquinoid geometry associated with a torsion angle of 11.9° (3.6° in ROHF-CI); the other ring has an aromatic geometry with a torsion angle of about 41.5° (54.6° in ROHF-CI). The description we obtain for the ring-centered polaron lattice in an isolated chain of ES can be sketched as follows.

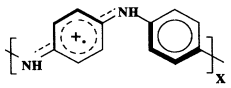

This differs from the representation usually adopted in the past which involved a nitrogen-centered polaron lattice:

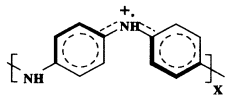

At this stage, it is difficult to determine which of these polaron lattice topologies is more stable and in better agreement with experimental results; packing effects and counterions do certainly significantly influence their relative stabilities.

2. *Electronic structure of the 50% p-doped LEB: Polaron lattice*

Using the unit cell discussed above for the ring-centered polaron lattice, we have calculated the VEH band structure of an isolated ES chain, Fig. 7. Again, as a consequence of the electron-hole asymmetry, the lower polaron band P_a (which is half filled) is clearly distinct from the rest of the valence band (it is located 0.96 eV above the valence band edge) while the upper polaron band P_b (empty) is only 0.16 eV below the conduction band edge. Thus we again find that only one polaronic band is well defined within the gap instead of the two bands found in the other conjugated polymers.

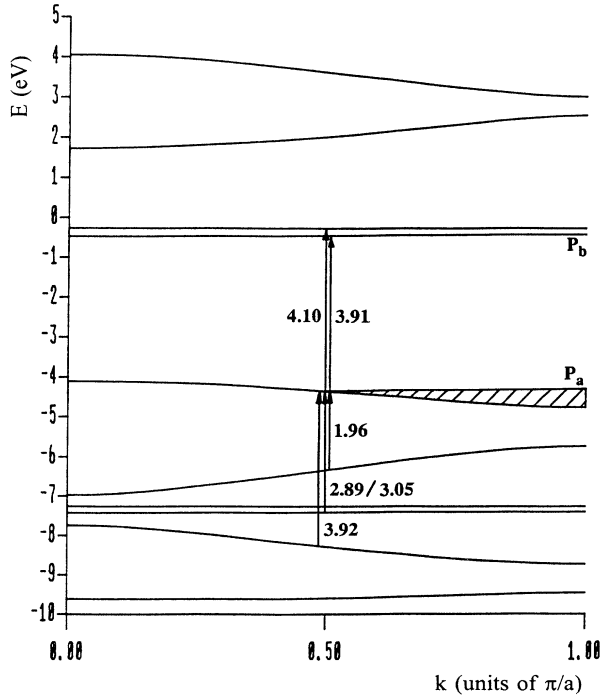

FIG. 7. VEH electronic band structure of the ring-centered polaron lattice (AM1-UHF) in emeraldine salt (50% *p*-doped leucoemeraldine).

The upper polaron band P_b is flat and the lower polaron band is 0.7 eV wide. The latter value is smaller than the experimental polaron bandwidth (1.0 eV).[10,11] This might be due to the fact that in our calculations no packing effects are considered; packing is expected to decrease the average torsion angles of the rings along the polymer chains [down to about $\pm 10°-15°$ (Refs. 25,37)], thereby increasing the π delocalization and the bandwidth of the lower polaronic band. If the ring torsion angles along the AM1-UHF optimized unit cell are fixed at $\pm 15°$, the calculated width for polaronic band P_a reaches 1.0 eV, while the VEH-calculated optical transitions remain basically unchanged.

From the VEH band structure, possible optical transitions are estimated at 1.96, 2.89, 3.05, 3.91, and 4.10 eV (see Fig. 7). Globally, there is a good agreement between the calculated values and the experimental values observed at 1.5, 3.0, and 3.8 eV,[46,47] except for the fact that the VEH lowest transition energy is overestimated by about 0.5 eV. However, it is interesting to note that a corresponding calculation for the nitrogen-centered polaron lattice leads to VEH-calculated transitions at 1.86, 2.95, 3.02, and 4.00–4.09 eV. The lowest optical transition is thus better described in this case.

We point out that with improved processing (crystallinity), the 1.5 eV absorption of ES is replaced by a "Drude-like" free-carrier tail extending to the far infrared. This is, for instance, the case in high-quality samples such as PANI-CSA salts (PANI protonated by camphor-sulfonic acid) cast from *m*-cresol solutions.[8]

It must be stressed that the separation between the valence and first polaron bands is much higher in the 50% *p*-doped LEB chain than in the 25% oxidized one; the reason for that is related to the fact that the average torsion-angle dimerization increases with the polaron concentration when we evolve from LEB to the ES oxidation state.

D. *p*-doped pentamer: Bipolaron formation

1. *RHF geometric and electronic structure of the (+2)-charged pentamer*

The AM1-RHF optimized geometry of the (+2)-charged oligomer is displayed in Table I. The +2 charge on the system leads to a significant deformation of the three inner phenyl rings and the adjacent C-N bonds (see $R1-R13$ in Table I), while the external rings are only slightly affected. The central phenyl ring and the C-N bonds connected to it (see $R1-R4$) present the largest deformations and adopt a strong semiquinoid geometry [r(C*p*-N)=1.345 Å, r(C*p*-C*o*)=1.453 Å, and r(C*o*-C*o*)=1.355 Å]. The neighboring phenyl rings ($C2$ and $C4$) and their adjacent C-N bonds present nonuniform alterations; it is the external side of these parts of the oligomer which is mostly affected (see $R10-R13$). Globally,

phenyl rings $C2$ and $C4$ and the adjacent C-N bonds gain a weaker semiquinoid character than is the case in the center of the pentamer.

The three inner rings, as a consequence of their semiquinoid structure, adopt more coplanar confirmations with respect to the nitrogen-atom plane. The evolution relative to the neutral case is more significant for the $C2$ and $C4$ rings than for the central ring; the external rings present large torsion angles. The dihedral angle between the central ring and its neighbors ($T1+|T2|$) decreases from 56.4° in the neutral pentamer to 38.2°; this induces an important increase of steric strains (strong diminution of $RHH1$) between these rings, partly compensated by a significant increase of the C-N-C angle $A1$ (the situation is just the opposite, though to a lesser extent, for the external rings).

The geometric structure obtained with the AM1-RHF technique for the (+2)-charged pentamer of LEB is in very good agreement with the x-ray diffraction data from Shacklette *et al.*[37] (see Fig. 8) on the same LEB oligomer, positively doped and complexed with BF_4^- anions. This confirms the reliability of the AM1 method in the context of our work.

The AM1-RHF net atomic charge distributions for the (+2)-charged pentamer are presented in Table II. The major part of the +2 charge is localized in the center of the oligomer. The central phenyl ring ($C3$) and the adjacent amine groups possess a positive charge gain of $+0.97|e|$ (note that the positive charge supported by the ring is slightly lower than for the adjacent amine sites). If we add the contributions from the neighboring rings ($C2$ and $C4$) and those of the connected amine sites, it gives a total of $+1.36|e|$, i.e., about 70% of the +2 charge. The positive charges are thus mainly localized in the center of the pentamer; the charge distributions are fully consistent with the geometric modifications discussed above and indicate the formation of a positive bipolaron defect, as found in the x-ray data of Shacklette *et al.*[37]

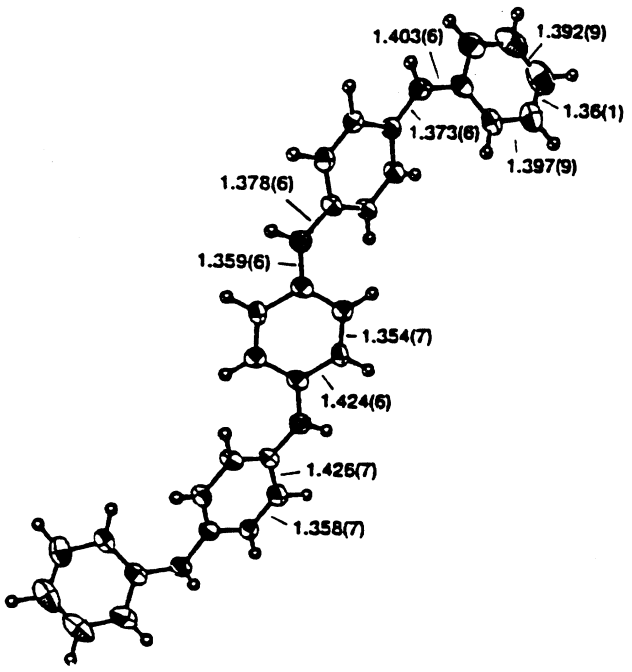

FIG. 8. X-ray structure (adapted from Ref. 37) of the LEB pentamer complexed with the BF_4^- anion; the bond lengths are in Å. The torsion angles (with respect to the plane of the nitrogen atoms) are 13.2° for the central phenyl ring and −17.1° for the neighboring rings.

The VEH oligomer results obtained from the (+2)-doped pentamer show that only one bipolaron level is introduced in the gap; this level is destabilized by 0.61 eV relative to the HOMO of the neutral case (0.54 eV for the phenyl-capped hexamer); this is similar to what is observed in the phenyl-capped PPV pentamer (0.58 eV). The transitions from the upper three occupied levels to the bipolaron level are calculated at 0.87, 1.72, and 2.83 eV, respectively.

It must be noted that the binding energy of the positive bipolaron in the pentamer (0.67 eV, AM1-RHF) is about three times larger than that of the positive polaron (0.22 eV, AM1-ROHF); it is not surprising that in the pentamer of LEB the bipolaron defect is more stable than two polarons, as is observed experimentally.[37] However, this positive bipolaron binding energy is considerably lower than the 1.01 eV (AM1-RHF value) obtained in the case of sexithiophene, i.e., the thiophene oligomer of similar size; in consequence, a positive bipolaron defect is less relaxed (or stable) in LEB than in polythiophene. The torsion-angle and bond-length contributions to the total relaxation (0.67 eV) induced upon (+2) doping are on the order of 20% and 80%, respectively; this is similar to the positive polaron case.

The AM1-RHF optimization of a (+2)-doped LEB hexamer leads to a bipolaron defect which is nitrogen centered, in contrast to the previous case. A more detailed theoretical study has shown that the topology of the bipolaron depends on the size of the oligomer and, more precisely, on the number of amine sites; the defect is nitrogen or ring centered when the oligomer contains odd or even number of amine sites, respectively; this holds true for chains with up to eight amine sites. This behavior (and its consequences on the electronic and geometric structure) will be addressed elsewhere.[48]

2. *Electronic structure of the 50% p-doped LEB: Bipolaron lattice*

If we extrapolate from the oligomer to the polymer chain, a ring-centered bipolaron extends over about three phenyl rings, the major semiquinoidlike deformations taking place in the center of the defect. The unit cell representative of the 50% p-doped LEB chain supporting a ring-centered positive bipolaron lattice therefore contains four -(NH-ring)-units, three of them being deformed by the bipolaron defect. The corresponding VEH band structure is illustrated in Fig. 9.

Two (totally empty) bipolaron bands can be considered as appearing within the gap; again, there is a strong asymmetry: the lower bipolaron band BP_a is 0.55 eV above the valence band edge and is narrow (0.14 eV wide) while the upper bipolaron band BP_b is totally flat and lo-

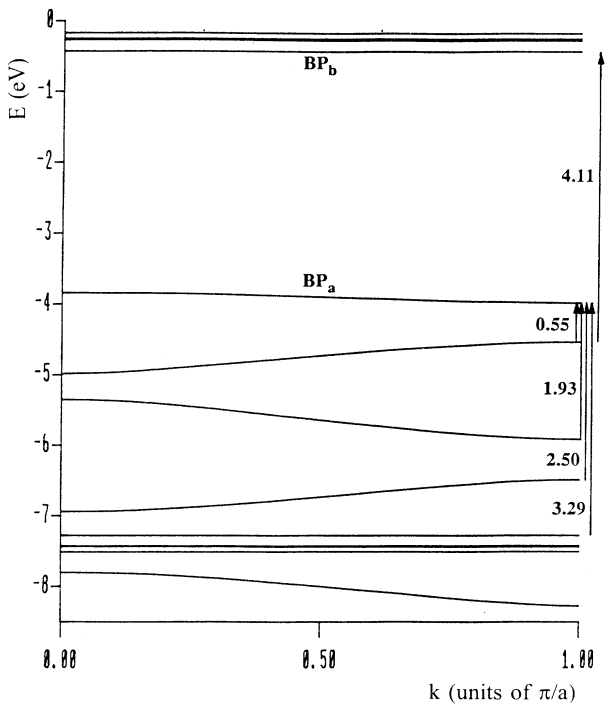

FIG. 9. VEH electronic band structure of the ring-centered bipolaron lattice in emeraldine salt.

cated 0.16 eV below the conduction band edge (we note that almost identical VEH results are obtained if we consider a nitrogen-centered bipolaron lattice). The semiconducting nature of the band structure calculated for the bipolaron lattice is not consistent with the high electrical conductivity observed for emeraldine salt. It must be noted that Stafström *et al.* have obtained similar results with a MNDO-optimized unit cell.[11]

At this stage, it is important to stress that it is very difficult computationally to estimate the energy difference between the polaron lattice and the bipolaron lattice. Indeed, the two-polaron situation and the bipolaron situation on the oligomer are treated by two approaches (UHF or ROHF-CI vs RHF, respectively) which provide different treatments of the electron-electron interaction correlation terms. The best we can do in the present context is to impose the formation of either a polaron or a bipolaron lattice and analyze the implications on the corresponding band structures; in that respect, only the polaron lattice is consistent with the metallic regime in emeraldine salt. Furthermore, we note that the stability difference between the two types of lattice can be influenced by subtle effects coming from the presence of counterions, interchain interactions, and disorder; these effects are not taken into account in the present calculations.

E. Singly charged *n*-doped pentamer

1. *Geometric and electronic structure of the (−1)-charged pentamer*

The AM1-ROHF optimized geometrical parameters of the (−1)-charged pentamer are presented in Table III. The geometric deformations induced by the introduction of the −1 charge are clearly less significant than for the positive polaron case. Small changes in bond lengths are observed for the central phenyl ring and the inner side of its neighboring rings (see $R6$ and $R7$ in Table III) as well as for C-N bonds $R5$, $R12$, and $R13$. The evolution towards a semiquinoidlike geometry is thus very weak and the rings present a dominant aromatic character; this is also exemplified by the fact that the torsion angles of the phenyl rings are almost unchanged. As a result, the negative defect is weakly bound to the lattice. This is in agreement with the results of SSH calculations for a negative polaron on a LEB chain assuming only torsion-angle effects.[22,23]

The AM1-ROHF binding energy of the singly negatively charged defect is 0.10 eV, a value which is about two times smaller than that for the positive polaron (0.22 eV) in the pentamer.

The AM1-ROHF net atomic charge distributions for the (−1)-charged pentamer are given in Table IV. The negative charge is distributed among the phenyl rings (principally on the inner rings), while the amine sites are hardly affected (and actually become slightly more posi-

TABLE III. Geometries in the neutral (AM1-RHF), (−1)-charged (AM1-ROHF), and (−2)-charged (AM1-RHF) states of the LEB pentamer. The modifications Δ relative to the neutral system are also indicated. The bond lengths (Rx) and the distances between the interacting hydrogen atoms ($RHHx$) are in Å. The bond angles and torsion angles (Ax and Tx) are in degrees. The labels are given in Fig. 1.

Parameter	Neutral (RHF)	−1 (ROHF)	Δ−1 (ROHF)	−2 (RHF)	Δ−2 (RHF)
$R1$	1.412	1.425	+0.013	1.434	+0.022
$R2$	1.386	1.373	−0.013	1.367	−0.019
$R3$	1.415	1.426	+0.011	1.433	+0.018
$R4$	1.396	1.396	0.000	1.383	−0.013
$R5$	1.397	1.374	−0.023	1.367	−0.030
$R6$	1.412	1.424	+0.012	1.435	+0.023
$R7$	1.415	1.430	+0.015	1.439	+0.024
$R8$	1.386	1.380	−0.006	1.372	−0.014
$R9$	1.386	1.378	−0.008	1.370	−0.014
$R10$	1.415	1.413	−0.002	1.421	+0.006
$R11$	1.411	1.414	+0.003	1.423	+0.012
$R12$	1.398	1.412	+0.014	1.405	+0.007
$R13$	1.394	1.377	−0.017	1.366	−0.028
$R14$	1.417	1.423	+0.005	1.433	+0.016
$R15$	1.415	1.419	+0.004	1.428	+0.013
$R16$	1.389	1.386	−0.003	1.379	−0.010
$R17$	1.391	1.391	0.000	1.386	−0.005
$R18$	1.393	1.393	0.000	1.398	−0.005
$R19$	1.395	1.393	−0.002	1.395	0.000
$T1$	26.4	27.8	+1.4	23.2	−3.2
$T2$	−30.0	−28.8	+1.2	−28.4	+1.6
$T3$	25.0	21.2	−3.8	18.1	−6.9
$A1$	125.5	126.2	+0.7	128.5	+3.0
$A2$	125.9	127.4	+1.5	129.1	+3.2
$RHH1$	2.323	2.344	+0.021	2.224	−0.099
$RHH2$	2.283	2.149	−0.134	2.082	−0.201

TABLE IV. Net atomic charge distributions for the neutral (AM1-RHF), (−1)-charged (AM1-ROHF), and (−2)-charged (AM1-RHF) states of the LEB pentamer. The modifications Δ relative to the neutral system are also indicated. All the net atomic charges are in $|e|$. The labels are given in Fig. 1.

Group	Neutral (RHF)	−1 (ROHF)	Δ−1 (ROHF)	−2 (RHF)	Δ−2 (RHF)
$C1$	0.028	−0.118	−0.146	−0.281	−0.309
$N1$	−0.071	−0.053	+0.018	−0.006	+0.065
$C2$	0.080	−0.174	−0.254	−0.480	−0.560
$N2$	−0.071	−0.029	+0.042	+0.053	+0.124
$C3$	0.070	−0.250	−0.320	−0.596	−0.666
$N3$	−0.071	−0.028	+0.043	+0.053	+0.124
$C4$	0.080	−0.175	−0.255	−0.480	−0.560
$N4$	−0.071	−0.054	+0.017	−0.006	+0.065
$C5$	0.028	−0.120	−0.148	−0.281	−0.309

tive). This evolution is consistent with the fact that the LUMO band of neutral leucoemeraldine base is entirely localized within the phenyl rings.

In order to obtain a refined description of this singly negative defect, we have also performed an AM1-ROHF optimization of a (−1)-charged LEB hexamer; in this case, the negative charge spreads over all the rings and there occurs a decrease in the amplitude of the geometric deformations. Thus, as the size of the system increases, the negative charge tends no longer to induce the formation of a polaron.

Oligomer VEH calculations performed on the (−1)-charged pentamer show that the first defect level is destabilized by only 0.10 eV with respect to the HOMO level of the neutral system; this value is about three times smaller than that observed for the positive polaron. The second defect level remains very close to the LUMO levels and is not stabilized even though it is half occupied; this is due to the fact that the associated wave function possesses nodes on the nitrogens and *para* carbon atoms (thereby inducing strong conjugation breaks). Transitions are calculated between the upper defect level and unoccupied levels; they occur in the ir range and around 1.2 and 2.4 eV.

2. *Electronic structure of the 25% n-doped LEB chain*

A four-ring unit cell, representative of the 25% n-doped LEB chain, is built from the AM1-ROHF geometry of the (−1)-charged pentamer; the VEH electronic band structure of the n-doped polymer is illustrated in Fig. 10. Since the geometry modifications with respect to the neutral case are extremely weak, the band structure is hardly modified except for the fact that the glide-plane symmetry is slightly lifted (which removes degeneracies at the center and edges of the first Brillouin zone). The upper doubly occupied band (band D in Fig. 10) lies 0.03 eV above the next valence band while the half-occupied band (band S) lies 0.04 eV below the conduction band. This is in agreement with the experiments of McCall *et al.*,[44] which suggest that the negative polaron levels remain close to the valence and conduction

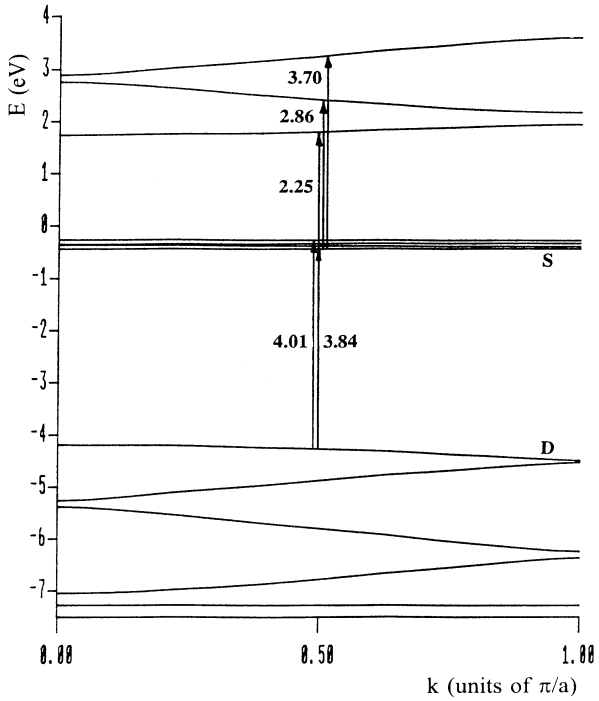

FIG. 10. VEH electronic band structure of the 25% n-doped LEB chain containing polarons.

band edges.[22,23] The D and S bands are narrow (0.31 eV) and very flat (0.01 eV), respectively. In view of these results, we expect the band structure not to be significantly modified even if the concentration in polarons increases up to 50% (i.e., the equivalent of the polaron lattice for the p-type doping case).

Several VEH transitions are calculated in the visible range at 2.25 and 2.86 eV, and at 3.70 eV. These all involve excitations from the S band to higher-lying unoccupied bands. Transitions between the D band and the lower unoccupied levels are found around 4.0 eV. Because none of the characteristics calculated at the VEH molecular and polymeric levels corresponds to the photoinduced features, it seems reasonable that the absorption peaks, which might be induced in the visible by a singly charged negative defect, must possess very weak oscillator strengths (this is confirmed by recent calculations at the INDO-CI level[49]). It must be noted that absorption spectra devoted to n-type doping of LEB have not been reported yet in the literature.

F. Doubly charged n-doped pentamer

1. *Geometric and electronic structure of the (−2)-charged pentamer (RHF)*

The AM1-RHF optimized geometrical of the (−2)-charged pentamer are presented in Table III. The deformations induced by the introduction of two negative charges into the system are weaker but more extended compared to the positive bipolaron case. Globally, defor-

mations in carbon-carbon bond lengths ranging between 0.01 and 0.03 Å are observed in going from the center to the internal sides of the terminal phenyl rings (see $R1-R16$). Note that the C-N bond lengths generally decrease, two of them being more affected ($R5$ and $R13$). The oligomer evolves towards a weak semiquinoid geometry, the tendency being stronger in the center.

The torsion angles of the three internal phenyl rings are weakly affected and decrease in absolute value. The external rings undergo larger modifications (by 6°–9°) and adopt a conformation more coplanar with the nitrogen-atom plane. The inner dihedral angles ($T1+|T2|$) are reduced by 4.8°, while the external ones ($|T2|+T3$) diminish more strongly (8.5°); this induces an increase in steric strain (see $RHH1$ and $RHH2$) compensated by a simultaneous widening of the C-N-C bond angles $A1$ and $A2$.

The AM1-RHF net atomic charge distributions for the (−2)-charged oligomer are collected in Table IV. As for the singly charged case, the phenyl rings are only sites where there occurs a negative charge gain (while the amine groups exhibit positive charge gains). The central phenyl ring acquires a 0.67 negative charge; the three inner rings and the amine units connecting them globally contain 77% of the −2 charge introduced on the oligomer. We can consider that a negative bipolaronlike defect is formed in this small oligomer; although it is more localized in the center of the oligomer, the defect extends significantly over all the rings and is less bound than a positive bipolaron. The AM1-RHF binding energy of the doubly negatively charged defect (0.26 eV) is indeed about 2.5 times smaller than for the positive bipolaron in the same LEB pentamer (0.67 eV).

We have also optimized (at the AM1-RHF level) a longer (−2)-charged LEB oligomer, in order to check the evolution of the localization of the negative charges as the size of the system increases; in order to do so, we have considered an octamer of LEB. We find that the excess charges spread homogeneously on all the inner phenyl rings of the oligomer and induce very weak geometric deformations (all the amine sites presenting a small positive charge gain). These results indicate that no negative bipolaron is formed on a LEB chain upon *n*-type doping. We have also optimized the AM1-RHF geometry of a polymer chain where the translation cell corresponds to a (−2)-charged -(NH-ring)$_8$- unit. In this case, which corresponds to a doping level of 12.5%, we obtain again that the negative charges spread over all the rings of the unit cell.

VEH oligomer results have been obtained for the (−2)-doped LEB pentamer and show that the first defect level is destabilized by only 0.26 eV relative to the HOMO level of the neutral case; it is less than for the positive bipolaron and even than for the positive polaron. The second defect level remains close to the LUMO level and is not stabilized even though it is doubly occupied; again, this must be related to the nature of the corresponding wave function, which possesses nodes on both nitrogen and *para* carbon sites. Transitions, which imply the upper defect level and unoccupied levels, are calculated to occur in the ir range and at about 1.1 and 2.3 eV.

2. *Electronic structure of the 50% n-doped LEB*

The VEH band structure of the 50% *n*-doped LEB chain (Fig. 11) is little different from that in the neutral situation, except for the filling of the lowest conduction band (D). This band remains totally flat and lies 0.09 eV below the empty bands. VEH transitions are calculated to occur at 2.23 and 2.41 eV and imply excitations from band D to higher unoccupied bands. Several transitions are also calculated in the range 4.02–4.14 eV. The flatness of the band in which excess electrons can be accommodated indicates that the mobility of these charges should be extremely low.

Because the oligomer and polymer VEH-calculated transitions have no correspondence in the photoinduced spectra of LEB, these features probably have very weak oscillator strengths.[49] Again, optical absorption data based on the *n*-type doping of LEB should give important information but, up to now, there are no such studies reported in the literature. Furthermore, the disorder present in the polymer may broaden these far-infrared transitions, making it difficult to observe them experimentally.

IV. SYNOPSIS

We have theoretically investigated, by using a combination of AM1 and VEH quantum-chemical techniques, the effects of *p*- and *n*-type doping on the geometric structure and electronic properties of the leucoemeraldine base polymer. Our results provide a detailed characterization of the different charge-storage

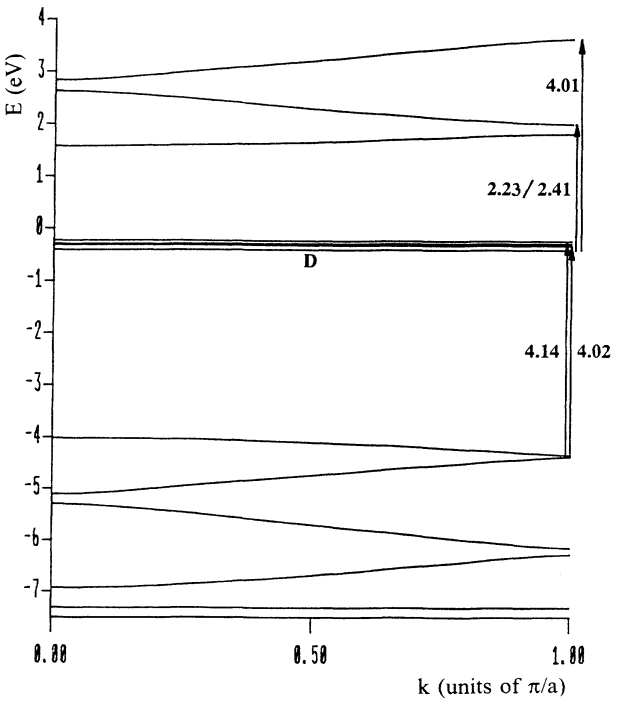

FIG. 11. VEH electronic band structure of the 50% *n*-doped LEB chain containing bipolarons.

species which can appear upon doping of this polymer. Leucoemeraldine supports positive polarons or bipolarons which can be N centered and/or ring centered and which induce geometry modifications towards a semiquinoid type of structure. Due to the very strong electron-hole asymmetry in leucoemeraldine base, different evolutions are found for p- and n-type doping.

From the geometry standpoint, positive charges lead to significant local lattice relaxations. The appearance of negative charges, on the contrary, result in weaker and more extended deformations. From the electronic structure standpoint, positive polarons or bipolarons induce a lower defect band which is well separated from the valence band edge while the upper defect band remains close to the conduction band edge. Our results allow for a simple interpretation of the positive polaron formation; they provide a refined description of the positive polaron lattice on an emeraldine salt chain (i.e., 50% oxidized LEB) where the unit cell can be represented as follows:

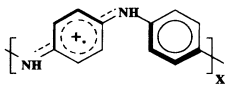

or

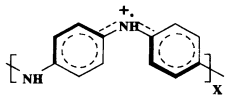

The local environment is the major factor which should determine which is the more stable of these two structures.

Upon n-type doping, the excess charges do not form significantly bound polaron or bipolaron defects; they induce weak deformations only within the phenyl rings. As a result, the band structure hardly evolves with respect to the neutral case (except for the filling).

ACKNOWLEDGMENTS

One of us (J. Libert) is supported by the Belgian "Institut pour l'Encouragement de la Recherche Scientifique dans l'Industrie et l'Agriculture" through a Ph.D. grant. The collaboration between Mons and Ohio State is supported by NATO Scientific Affairs Division (Collaborative Research Grant No. 242/089). The conjugated polymer work in Mons is partly supported by the Belgian Prime Minister Office of Science Policy "Programme d'Impulsion en Technologie de l'Information (contrat IT/SC/22)" and "Pôle d'Attraction Interuniversitaire en Chimie Supramoléculaire et Catalyse," the Belgian National Fund for Scientific Research (FNRS/FRFC), and an IBM Academic Joint Study; it is conducted in the framework of the European Commission ESPRIT Network of Excellence on Organic Materials for Electronics (NEOME) and Human Capital and Mobility Networks.

[1]J.-C. Chiang and A. G. MacDiarmid, Synth. Met. **13**, 193 (1986).

[2]A. G. MacDiarmid, J.-C. Chiang, A. F. Richter, N. L. D. Somasiri, and A. J. Epstein, in *Conducting Polymers,* edited by L. Alcacer (Reidel, Dordrecht, 1987), p. 105.

[3]E. M. Genies, A. Syed, and C. Tsintavis, Mol. Cryst. Liq. Cryst. **121**, 181 (1985).

[4]J. P. Travers, J. Chroboczek, F. Devreux, F. Genoud, M. Nechtshein, A. Syed, E. M. Genies, and C. Tsintavis, Mol. Cryst. Liq. Cryst. **121**, 195 (1985).

[5]*Intrinsically Conducting Polymers: An Emerging Technology,* edited by M. Aldissi, NATO Advanced Study Institute Series E: Applied Sciences, Vol 246 (Kluwer, Dordrecht, 1992).

[6]A. G. MacDiarmid and A. J. Epstein, J. Chem. Soc. Faraday Trans. **88**, 317 (1989).

[7]A. G. MacDiarmid and A. J. Epstein, in *Advanced Organic Solid State Materials,* edited by L. Y. Chiang, P. M. Chaikin, and D. O. Cowan, MRS Symposia Proceedings No. 173 (Materials Research Society, Pittsburgh, 1990), p. 283.

[8]Y. Cao, P. Smith, and A. J. Heeger, Synth. Met. **48**, 91 (1992); M. Reghu, Y. Cao, D. Moses, and A. J. Heeger, Phys. Rev. B **47**, 1758 (1993); N. S. Sariciftci, A. J. Heeger, and Y. Cao, *ibid.* **49**, 5988 (1994); A. G. MacDiarmid and A. J. Epstein, *Proceedings of the Second Brazilian Polymer Conference I, São Paulo, 1993* (Plenum, New York, 1993); p. 554; J. Joo, Z. Oblakowski, G. Du, J. Pouget, E. J. Oh, J. M. Weisinger, Y. Min, A. G. MacDiarmid, and A. J. Epstein, Phys. Rev. B **49**, 2977 (1994).

[9]A. G. MacDiarmid, J.-C. Chiang, A. F. Richter, and A. J. Epstein, Synth. Met. **18**, 285 (1987); A. J. Epstein, J. M. Ginder, F. Zuo, R. W. Bigelow, H. S. Woo, D. B. Tanner, A. F. Richter, W. S. Wang, and A. G. MacDiarmid, *ibid.* **18**, 303 (1987).

[10]J. M. Ginder, A. F. Richter, A. G. MacDiarmid, and A. J. Epstein, Solid State Commun. **63**, 97 (1987).

[11]S. Stafström, J. L. Brédas, A. J. Epstein, H. S. Woo, D. B. Tanner, W. S. Huang, and A. G. MacDiarmid, Phys. Rev. Lett. **59**, 1464 (1987).

[12]G. E. Wnek, Polym. Prepr. Am. Chem. Soc. Div. Polym. Chem. **27**, 277 (1986).

[13]*Handbook of Conducting Polymers,* edited by T. A. Skotheim (Dekker, New York, 1986).

[14]*Conjugated Polymers: The Novel Science and Technology of Highly Conducting and Nonlinear Optically Active Materials,* edited by J. L. Brédas and R. Silbey (Kluwer, Dordrecht, 1991).

[15]A. Ray, G. E. Astruias, D. L. Kershner, A. F. Richter, A. G. MacDiarmid, and A. J. Epstein, Synth. Met. **29**, E141 (1989).

[16]E. W. Paul, A. J. Ricco, and M. S. Wrighton, J. Phys. Chem. **89**, 1441 (1985).

[17]T. Ohsawa, T. Kabata, O. Kimura, and K. Yoshino, Synth. Met. **29**, E203 (1989).

[18]J. M. Ginder, A. J. Epstein, and A. G. MacDiarmid, Synth. Met. **29**, E395 (1989); A. J. Epstein and A. G. MacDiarmid, in *Advanced Organic Solid State Materials* (Ref. 7), p. 293.

[19]J. L. Brédas, in *Conjugated Polymers and Related Materials: The Interconnection of Chemical and Electronic Structure,* edited by W. R. Salaneck, I. Lundström, and B. Rånby (Oxford University Press, Oxford, 1992), p. 187.

[20]S. Stafström and J. L. Brédas, Synth. Met. **14**, 297 (1986).

[21]A. J. Epstein, J. M. Ginder, A. F. Richter, and A. G. MacDiarmid, in *Conducting Polymers* (Ref. 2), p. 121.

[22]J. M. Ginder, A. J. Epstein, and A. G. MacDiarmid, Solid State Commun. **72**, 987 (1989).
[23]J. M. Ginder and A. J. Epstein, Phys. Rev. B **41**, 10 674 (1990).
[24]J. G. Masters, J. M. Ginder, A. G. MacDiarmid, and A. J. Epstein, J. Chem. Phys. **96**, 4768 (1992).
[25]J. P. Pouget, M. E. Jozefowicz, A. J. Epstein, X. Tang, and A. G. MacDiarmid, Macromolecules **24**, 779 (1991).
[26]J. L. Brédas, C. Quattrochhi, J. Libert, A. G. MacDiarmid, J. M. Ginder, and A. J. Epstein, Phys. Rev. B **44**, 6002 (1991).
[27]R. P. McCall, J. M. Ginder, M. G. Roe, G. E. Asturias, E. M. Scherr, A. G. MacDiarmid, and A. J. Epstein, Phys. Rev. B **39**, 10 174 (1989); R. P. McCall, J. M. Ginder, and A. J. Epstein, Opt. Mem. Neural Networks **1**, 113 (1992).
[28]R. P. McCall, J. M. Ginder, J. M. Leng, K. A. Coplin, H. J. Ye, A. J. Epstein, G. E. Asturias, S. K. Manohar, J. G. Masters, E. M. Scherr, Y. Sun, and A. G. MacDiarmid, Synth. Met. **41–43**, 1329 (1991).
[29]J. M. Leng, J. M. Ginder, R. P. MacCall, H. J. Ye, Y. Sun, S. K. Manohar, A. G. MacDiarmid, and A. J. Epstein, Phys. Rev. Lett. **68**, 1184 (1992).
[30]M. J. S. Dewar, E. G. Zoebish, E. F. Healy, and J. J. P. Stewart, J. Am. Chem. Soc. **107**, 3092 (1985).
[31]M. J. S. Dewar and Y-C Yuan, Inorg. Chem. **29**, 3881 (1990).
[32]M. J. S. Dewar and W. Thiel, J. Am. Chem. Soc. **99**, 4899 (1977).
[33]M. J. S. Dewar and W. Thiel, J. Am. Chem. Soc. **99**, 4907 (1977).
[34]L. Salem, *Molecular Orbital Theory of Conjugated Systems* (Benjamin, New York, 1966).
[35]J. L. Rivail, *Eléments de Chimie Quantique à l'Usage des Chimistes* (Interéditions, Paris, 1989).
[36]D. R. Armstrong, P. G. Perkins, and J. J. P. Stewart, J. Chem. Soc. Faraday Trans. 2 **68**, 1839 (1972).
[37]L. W. Shacklette, J. F. Wolf, S. Gould, and R. H. Baughman, J. Chem. Phys. **88**, 3955 (1988).
[38]J. M. André, L. A. Burke, J. Delhalle, G. Nicolas, and Ph. Durand, Int. J. Quantum Chem. Symp. **13**, 283 (1979).
[39]J. L. Brédas, R. R. Chance, R. Silbey, G. Nicolas, and Ph. Durand, J. Chem. Phys. **75**, 255 (1981).
[40]H. Bässler (personal communication).
[41]J. L. Brédas and G. B. Street, Acc. Chem. Res. **18**, 309 (1985).
[42]M. E. Jozefowicz, A. J. Epstein, J. P. Pouget, J. G. Masters, A. Ray, Y. Sun, X. Tang, and A. G. MacDiarmid, Synth. Met. **41**, 723 (1991).
[43]D. S. Boudreaux, R. R. Chance, J. F. Wolf, L. W. Shacklette, J. L. Brédas, B. Thémans, J. M. André, and R. Silbey, J. Chem. Phys. **85**, 4584 (1986).
[44]R. P. McCall, J. M. Ginder, J. M. Leng, H. J. Ye, S. K. Manohar, J. G. Masters, G. E. Asturias, A. G. MacDiarmid, and A. J. Epstein, Phys. Rev. B **41**, 5202 (1990).
[45]*Handbook of Chemistry and Physics,* 69th ed., edited by R. C. Weast (CRC, Boca Raton, 1988–1989), p. D-188.
[46]A. J. Epstein, J. Joo, R. S. Kohlman, A. G. MacDiarmid, J. M. Weisinger, Y. Min, J. P. Pouget, and J. Tsukamoto, in *Electrical, Optical, and Magnetic Properties of Organic Solid State Materials,* edited by A. F. Garito, A. K. -Y. Jen, C. Y-C. Lee, L. R. Dalton, and C. Lee, MRS Symposia Proceedings No. 328 (Materials Research Society, Pittsburgh, 1994), p. 145.
[47]R. J. Cushman, P. M. McManus, and S. Z. Yang, Makromol. Chem. Rapid Commun. **8**, 69 (1987); A. P. Monkman, D. Bloor, G. C. Stevens, J. C. H. Stevens, and P. Nilson, Synth. Met. **29**, E277 (1989).
[48]J. Libert, J. L. Brédas, and A. J. Epstein (unpublished).
[49]J. Cornil, J. Libert, and J. L. Brédas (unpublished).